Magnetically catalyzed fusion

Jeremy S. Heyl and Lars Hernquist
Lick Observatory, University of California, Santa Cruz, California 95064
(Received 10 June 1996)

We calculate the reaction cross sections for the fusion of hydrogen and deuterium in strong magnetic fields as are believed to exist in the atmospheres of neutron stars. We find that in the presence of a strong magnetic field ($B \gtrsim 10^{12}$ G), the reaction rates are many orders of magnitude higher than in the unmagnetized case. The fusion of both protons and deuterons is important over a neutron star's lifetime for ultrastrong magnetic fields ($B \sim 10^{16}$ G). The enhancement may have dramatic effects on thermonuclear runaways and bursts on the surfaces of neutron stars. [S0556-2813(96)05611-7]

PACS number(s): 26.60.+c, 32.60.+i, 97.10.Ld, 97.60.Jd

I. INTRODUCTION: ATOMIC STRUCTURE IN AN INTENSE MAGNETIC FIELD

In large magnetic fields a hydrogen atom is compressed both perpendicular and parallel to the field direction. In a sufficiently strong magnetic field ($B \gtrsim 10^{12}$ G), the Schrödinger equation for the dynamics of the electron separates into axial and perpendicular (azimuthal and radial) equations. As the potential is axisymmetric around the direction of the magnetic field, we expect no azimuthal dependence in the ground-state wave function of the electron.

In the direction perpendicular to the magnetic field, the wave function can be obtained exactly [1]. This azimuthal wave function is denoted by two quantum numbers n and m. Here we take $n=0$, as the $n>0$ solutions are less bound and therefore provide less shielding.

The perpendicular wave function has the same form as the Landau wave function for an electron in a magnetic field:

$$R_{0m}(\rho,\theta)=\frac{1}{\sqrt{2^{m+1}\pi m!\,a_H^{m+1}}}\rho^m \exp\left(-\frac{\rho^2}{4a_H^2}\right)e^{im\theta}, \quad (1)$$

$$R_{0m}^2(\rho)=\frac{(-1)^m}{2\pi m!}\frac{1}{a_H^2}\left(\frac{d}{d\beta^m}\right)^m\left[\exp\left(-\beta\frac{\rho^2}{2a_H^2}\right)\right]\Bigg|_{\beta=1}, \quad (2)$$

where

$$a_H=\sqrt{\hbar/m_e\omega_H}=\sqrt{\hbar c/|e|H}. \quad (3)$$

A. Axial wave function

Along the direction of the magnetic field, the electron experiences an effective potential

$$V_{\mathrm{eff},0m}(z)=\langle R|V(r)|R\rangle=\int_0^\infty -\frac{e^2}{\sqrt{z^2+\rho^2}}R_{0m}^2(\rho)2\pi\rho d\rho. \quad (4)$$

Performing the integral yields

$$V_{\mathrm{eff},0m}(z)=-\frac{e^2}{a_H}\sqrt{\pi/2}\frac{(-1)^m}{m!}\left(\frac{d}{d\beta}\right)^m \times\left[\frac{1}{\sqrt{\beta}}\exp(\beta z^2/2a_H^2)\ \mathrm{erfc}(\sqrt{\beta}|z|/\sqrt{2}a_H)\right]\Bigg|_{\beta=1}, \quad (5)$$

which for large z approaches $-e^2/z$. The Schrödinger equation with this potential is not analytically solvable. We can note certain features of the desired solution. Because V_{eff} is everywhere finite, both the wave function and its first derivative must be continuous. Rather than solve the equation directly, we use a variational principle, which constrains the ground-state wave function ($\nu=0$) along the magnetic field for the given values of n and m. The index ν counts the number of nodes in the axial wave function. As with the $n>0$ states, the $\nu>0$ states are barely bound compared to the $\nu=0$ state.

Looking at the radial wave function, we take the wave function along the z axis to be a Gaussian as well:

$$Z(z)=\frac{1}{\sqrt[4]{2\pi}\sqrt{a_z}}\exp\left(-\frac{z^2}{4a_z^2}\right). \quad (6)$$

We must minimize the integral

$$I=\langle Z|H_{\mathrm{eff}}|Z\rangle=\int_{-\infty}^{\infty}[(\hbar^2/2m_e)(\nabla_z Z)^2+V_{\mathrm{eff}}Z^2]dz. \quad (7)$$

For this problem the integral is (using the definition of Z and $m=0$)

$$I=2\int_0^\infty Z^2\left[\frac{\hbar^2}{2m_e}\frac{a_H^3u^2}{4a_z^4}-e^2\sqrt{\pi/2}\exp(u^2/2)\ \mathrm{erfc}(u/\sqrt{2})\right]du, \quad (8)$$

where we have substituted $u=z/a_H$. Next, we use the definition of Z,

TABLE I. The results of the minimization.

	Ruder *et al.*		Our results			
B (G)	$E_{m=0}$ (Ry)	$E_{m=1}$ (Ry)	$\alpha_{m=0}$	$E_{m=0}$ (Ry)	$\alpha_{m=1}$	$E_{m=1}$ (Ry)
4.7×10^{9}	2.04	1.20	1.14	1.77	1.59	1.15
4.7×10^{10}	4.43	2.93	2.00	4.18	2.65	2.85
4.7×10^{11}	9.45	6.69	3.79	8.91	4.79	6.44
4.7×10^{12}	18.6	13.9	7.77	17.1	9.35	13.0
4.7×10^{13}			17.3	29.6	20.0	23.6
4.7×10^{14}			38.1	47.0	46.1	38.1
4.7×10^{15}			102.	69.6	113.0	59.1
4.7×10^{16}			265.	97.7	288.0	84.8

$$I=2\left[\frac{\hbar^2}{2m_e}\frac{a_H^3}{4\sqrt{2\pi}a_z^5}\int_0^\infty u^2\exp\left(-\frac{u^2a_H^2}{2a_z^2}\right)du - \frac{e^2}{2a_z}\int_0^\infty \exp(u^2/2)\exp\left(-\frac{u^2a_H^2}{2a_z^2}\right)\operatorname{erfc}(u/\sqrt{2})du\right]. \tag{9}$$

The first integral is tractable yielding the quantity to be minimized,

$$I=2\left[\frac{\hbar^2}{16m_ea_H^2}\frac{1}{\alpha^2}-\frac{e^2}{2a_H}\frac{1}{\alpha}\int_0^\infty \exp\left(\frac{u^2}{2}(1-1/\alpha^2)\right)\times\operatorname{erfc}(u/\sqrt{2})du\right], \tag{10}$$

with respect to $\alpha=a_z/a_H$. This minimization yields a value of a_z. Table I lists the results for the minimization for several magnetic field strengths and compares them with the eigenvalues for the energy of the bound state derived by Ruder *et al.* [2]. Ruder *et al.*use a series of basis functions to solve the Schrödinger equation.

Our binding energies fall short of theirs by approximately 20%, because we are restricted by our trial wave function. We also tried a sum of Gaussians but this added degree of freedom did not yield significantly more tightly bound wave functions.

Using the results of the minimization, the electron probability density is

$$\rho(r,z)=\frac{1}{a_H^2a_z(2\pi)^{3/2}}\exp\left[-\left(\frac{r^2}{2a_H^2}+\frac{z^2}{2a_z^2}\right)\right], \tag{11}$$

where we have combined the two Gaussians in a revealing fashion. The quadrupole moment of the distribution is given by $Q=2a_H^2(\alpha^2-1)$. Next we define a quantity

$$n^2=r^2+\left(\frac{a_H}{a_z}\right)^2z^2=r^2+\frac{z^2}{\alpha^2} \tag{12}$$

and recast the previous equation into the form

$$\rho(r,z)=\frac{1}{a_H^2a_z(2\pi)^{3/2}}\exp\left(-\frac{n^2}{2a_H^2}\right). \tag{13}$$

B. Screening potential

When solving gravitational problems one often looks for electrostatic analogs. Here, we look for a gravitational analog to an electrostatic problem. The density of the electron is constant on concentric, similar homoemoids. For this density distribution the potential is directly solvable [3],

$$\Phi(\vec{x})=-\pi G\left(\frac{a_2a_3}{a_1}\right)\int_0^\infty\frac{\psi(\infty)-\psi(m)}{\sqrt{(\tau+a_1^2)(\tau+a_2^2)(\tau+a_3^2)}}d\tau, \tag{14}$$

where we have the following auxiliary definitions:

$$m^2=a_1^2\sum_{i=1}^{3}\frac{x_i^2}{a_i^2+\tau} \tag{15}$$

and

$$\psi(m)=\int_0^{m^2}\rho(m^2)dm^2. \tag{16}$$

In our case, we use $G=-e^2$, $a_1=a_2=a_H$, $a_3=a_z$, and

$$\psi(m)=\frac{1}{a_z\pi\sqrt{2\pi}}\left[1-\exp\left(-\frac{m^2}{2a_H^2}\right)\right]. \tag{17}$$

Substituting these results into Eq. (14) yields

$$\Phi(\vec{x})=\frac{1}{\sqrt{2\pi}}e^2\times\int_0^\infty\frac{\exp\{-\frac{1}{2}[r^2/(a_H^2+\tau)+z^2/(a_z^2+\tau)]\}}{(\tau+a_H^2)\sqrt{\tau+a_z^2}}d\tau. \tag{18}$$

We change variables to simplify the integral. Using the natural units of the problem, we let $\overline{r}=r/a_H$, $\overline{z}=z/a_H$, and $u=\tau/a_H^2$. This gives the new equation

$$\Phi(\vec{x}) = \frac{e^2}{a_H}\frac{1}{\sqrt{2\pi}} \times \int_0^\infty \frac{\exp\{-\frac{1}{2}[\overline{r^2}/(1+u)+\overline{z^2}/(\alpha^2+u)]\}}{(1+u)\sqrt{\alpha^2+u}}du, \tag{19}$$

where we again use the previous definition of α. The potential at the center of the electron cloud ($r=0,\ z=0$) is given by

$$\Phi(0,0) = \frac{e^2}{a_H}\frac{2}{\sqrt{2\pi}}\frac{\ln(\alpha+\sqrt{\alpha^2-1})}{\sqrt{\alpha^2-1}}. \tag{20}$$

Moving away from the origin a change of variables is useful when evaluating the integral. Let

$$v = \frac{1}{1+u}. \tag{21}$$

The integral becomes

$$\Phi(\vec{x}) = \frac{1}{\sqrt{2\pi}}\frac{e^2}{a_H} \times \int_0^1 \frac{\exp(-\frac{1}{2}\{\overline{r^2}v+\overline{z^2}v/[1+(\alpha^2-1)v]\})}{\sqrt{(\alpha^2-1)v^2+v}}dv. \tag{22}$$

As an example we present results for $B=9.8\times10^{12}$ G. For this field strength $a_H \approx 10^{-12}$ m and $a_z \approx 10^{-11}$ m, and so $\alpha=10$. The range of the nuclear force is approximately 10^{-15} m or $0.001a_H$. Figure 1 depicts the potential in units of e^2/a_H for this configuration. The central potential is approximately $0.25e^2/a_H$ and drops quickly in the radial direction. In the axial direction, the potential forms a ''core.''

The total potential of the electron cloud and the proton may be approximated by the quadrupole formula

$$V(\vec{x}) \approx -\frac{\alpha^2-1}{2}\frac{ea_H^2}{r^3}(3\cos^2\phi-1) \tag{23}$$

for large separations.

C. Cloud-cloud potential

When we consider the interaction between the two electron clouds surrounding the protons, we must account not only for their electrical potential but also the antisymmetry of the mutual electron wave function. Because of the strong ambient field, we expect that both electron spins will be aligned with the field, and so the spatial component of the wave function must be antisymmetric. That is,

$$\Psi(\vec{x}_1,\vec{x}_2) = \frac{1}{\sqrt{2}}[\psi_1(\vec{x}_1)\psi_2(\vec{x}_2)-\psi_1(\vec{x}_2)\psi_2(\vec{x}_1)], \tag{24}$$

where

$$\psi_1(\vec{x}) = \sqrt{\rho(\vec{x})} \quad \text{and} \quad \psi_2(\vec{x}) = \psi_1(\vec{x}-\vec{x}_0), \tag{25}$$

with $\rho(\vec{x})$ given by Eq. (11) and $\vec{x}_0$ is the position of the center of the second electron cloud.

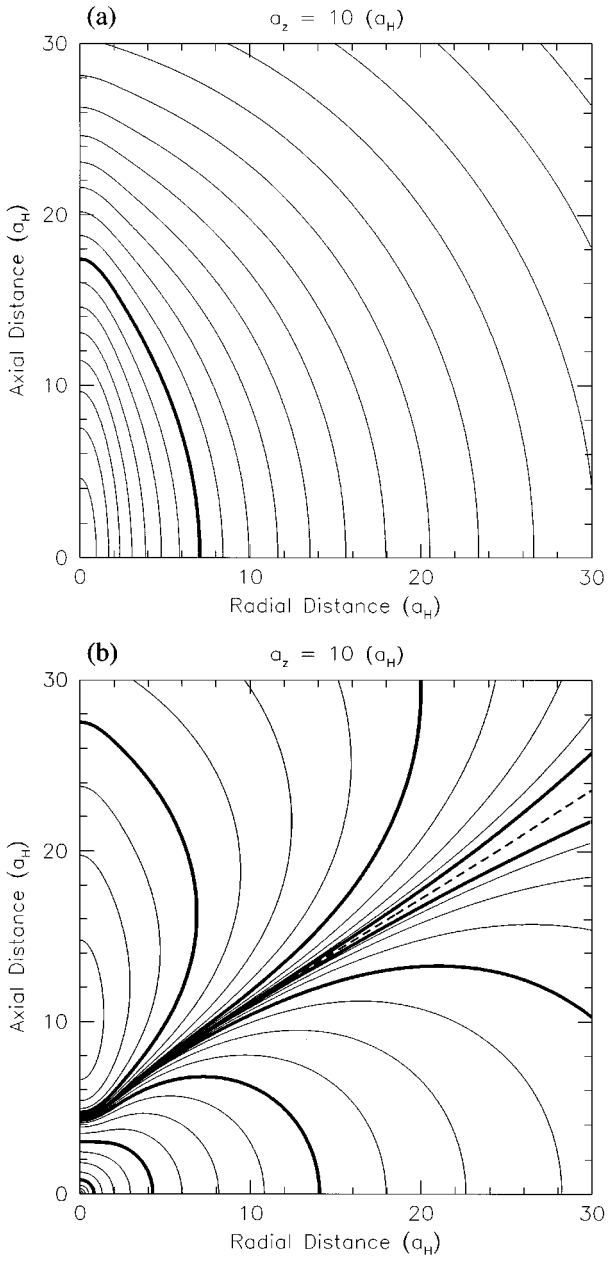

FIG. 1. The left panel depicts the screening potential as a function of radius and z position. The right panel shows the total potential experienced by an incoming proton. The dashed contour denotes zero potential. The other contours are logarithmically spaced. In the left panel the bold contour traces a potential of $0.1e^2/a_H$. The contour levels increase toward the center with a spacing of $10^{1/20}$. In the right panel the bold contours trace potentials of $\pm10^{-4}, 10^{-3}, \ldots, e^2/a_H$.

The potential energy of the two electrons is given by (e.g., [4])

$$\Phi_{cc}(\vec{x}_0) = \int\int \frac{e^2}{|\vec{x}_1-\vec{x}_2|}|\Psi(\vec{x}_1,\vec{x}_2)|^2 d^3x_1 d^3x_2 \tag{26}$$

$$= A(\vec{x}_0) - J(\vec{x}_0), \tag{27}$$

where $A(\vec{x}_0)$ and $J(\vec{x}_0)$ are given by

$$A(\vec{x}_0)=\int\int \frac{e^2}{|\vec{x}_1-\vec{x}_2|}\rho_1(\vec{x}_1)\rho_2(\vec{x}_2)d^3x_1d^3x_2\,, \tag{28}$$

$$J(\vec{x}_0)=\int\int d^3x_1d^3x_2\left\{\frac{e^2}{|\vec{x}_1-\vec{x}_2|}\rho_1(\vec{x}_1)\rho_2(\vec{x}_2)\exp\left[-\frac{1}{2}\left(\frac{(x_1-x_2)x_0+(y_1-y_2)y_0}{a_H^2}+\frac{(z_1-z_2)z_0}{a_z^2}\right)\right]\right\} \tag{29}$$

$$\approx\int\int d^3x_1d^3x_2\left\{\frac{e^2}{|\vec{x}_1-\vec{x}_2|}\rho_1(\vec{x}_1)\rho_2(\vec{x}_2)\exp\left[-\frac{1}{2}\left(\frac{x_0^2+y_0^2}{a_H^2}+\frac{z_0^2}{a_z^2}\right)\right]\right\} \tag{30}$$

$$\approx A(\vec{x}_0)\exp\left[-\left(\frac{r_0^2}{2a_H^2}+\frac{z_0^2}{2a_z^2}\right)\right], \tag{31}$$

where we have used the Gaussian form of $\rho(\vec{x})$ to simplify the expression for $J(\vec{x}_0)$, and to obtain its approximate value we replace x_1-x_2 by x_0 and similarly for the other coordinates.

To calculate the direct term of cloud-cloud potential $[A(\vec{x}_0)]$ we will take advantage of the special form of the density distribution given in Eq. (11). The direct term is in general given by

$$A(\vec{x}_0)=\int d^3x_1\rho(\vec{x}_1-\vec{x}_0)\Phi(\vec{x}_1), \tag{32}$$

which is simply the convolution of the density distribution with the potential. If we perform the Fourier transform of the right-hand side, we get

$$A(\vec{x}_0)=\int d^3k\widetilde{\rho}(\vec{k})\widetilde{\Phi}(\vec{k})e^{-i\vec{k}\cdot\vec{x}_0}. \tag{33}$$

Expressing the Poisson equation in Fourier space gives

$$\Phi(\vec{x})=-4\pi\int\frac{d^3k}{(2\pi)^{3/2}}\frac{\widetilde{\rho}(\vec{k})}{k^2}e^{-i\vec{k}\cdot\vec{x}}. \tag{34}$$

Because the magnetic field induces the deformation of both electron clouds, the clouds are aligned, and they have the same Fourier transforms; therefore,

$$A(\vec{x}_0)=-4\pi\int d^3k\frac{[\widetilde{\rho}(\vec{k})]^2}{k^2}e^{-i\vec{k}\cdot\vec{x}_0}. \tag{35}$$

Because ρ is a three-dimensional Gaussian, so is its Fourier transform; consequently,

$$[\widetilde{\rho}(\vec{k})]^2=\frac{1}{(2\pi)^{3/2}}\widetilde{\rho}(\sqrt{2}\vec{k}). \tag{36}$$

Combining Eq. (35) and Eq. (36), yields

$$A(\vec{x}_0)=-4\pi\frac{1}{(2\pi)^{3/2}}\int d^3k\frac{\widetilde{\rho}(\sqrt{2}\vec{k})}{k^2}e^{-i\vec{k}\cdot\vec{x}_0}. \tag{37}$$

Performing a change of variables $\vec{l}=\sqrt{2}\vec{k}$ gives

$$A(\vec{x}_0)=-4\pi\frac{1}{\sqrt{2}(2\pi)^{3/2}}\int d^3l\frac{\widetilde{\rho}(\vec{l})}{l^2}e^{-i\vec{l}\cdot\vec{x}_0/\sqrt{2}}. \tag{38}$$

Comparing this equation with Eq. (34), we get

$$A(\vec{x}_0)=\frac{1}{\sqrt{2}}\Phi\left(\frac{\vec{x}_0}{\sqrt{2}}\right). \tag{39}$$

Therefore, the total potential energy between two hydrogen atoms separated by $\vec{x}$ in the magnetic field is given by

$$V(\vec{x})\approx\frac{e^2}{r}+\frac{1}{\sqrt{2}}\Phi\left(\frac{\vec{x}}{\sqrt{2}}\right)\left\{1-\exp\left[-\left(\frac{r^2}{2a_H^2}+\frac{z^2}{2a_z^2}\right)\right]\right\}-2\Phi(\vec{x}), \tag{40}$$

where $\Phi(\vec{x})$ is simply the potential induced by the Gaussian cloud of charge [Eq. (22)].

Far from the atoms ($r\gg\alpha a_H$), the interaction energy may be approximated by the quadrupole-quadrupole energy

$$V(\vec{x})\approx\frac{3}{4}(\alpha^2-1)^2\frac{e^2a_H^4}{r^5}(35\cos^4\phi-30\cos^2\phi+3), \tag{41}$$

where ϕ is the angle relative to the symmetry axis of the atom.

Figures 2 and 3 depict the total potential energy between two hydrogen atoms in a magnetic field for the same magnetic-field strength as Fig. 1 ($B=9.8\times10^{12}$ G). A comparison of the two figures illustrates that the exchange term provides a slight attractive force between the two electron clouds, because of the anticorrelation of the clouds. At large separations, both potentials are well approximated by the quadrupole-quadrupole formula [Eq. (41)].

II. ESTIMATING REACTION RATES

In a fluid state, there will be three possible reaction channels: (i) proton-proton dominates in hot, totally ionized gas, (ii) proton-atom dominates in nearly completely ionized gas,

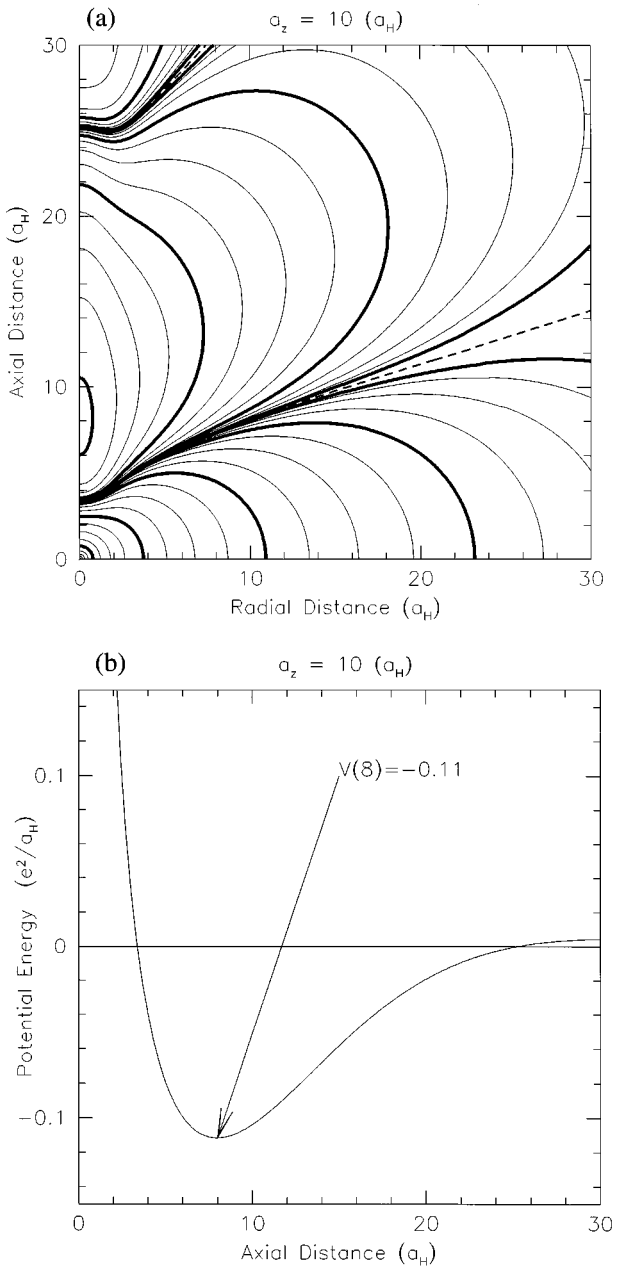

FIG. 2. The figures depict the total potential energy between two magnetized hydrogen atoms excluding the antisymmetrization energy. For the left panel, the contour spacing is the same as in the right panel of Fig. 1. The right panel illustrates the potential along the axis of the magnetic field.

and (iii) atom-atom dominates in neutral and partially ionized gas. For the first channel, we can use the standard thermonuclear reaction rates (e.g., [5]). For the latter two channels we must include the screening potentials that we calculated in the previous section to determine the potential wall through which the interacting particles must penetrate.

A. Transmission probability

In the WKB approximation, the probability to traverse through a potential wall is

$$|T|^2 \approx \exp\left(-2\int_{\text{wall}} dr\,\sqrt{\frac{2m}{\hbar^2}(V(r)-E)}\right) \tag{42}$$

$$\approx \exp\left(-2\sqrt{2ma_H}\frac{e}{\hbar}\int_{\text{wall}} du\,\sqrt{\frac{V(r)-E}{e^2/a_H}}\right) \tag{43}$$

$$\approx \exp\left(-26.69B_{12}^{-1/4}\int_{\text{wall}} du\,\sqrt{\mathcal{V}(u)-\mathcal{E}}\right), \tag{44}$$

where B_{12} is the magnetic-field strength in units of 10^{12} G, u is the dimensionless radius r/a_H, and $\mathcal{E}$ and $\mathcal{V}$ are the dimensionless energy Ea_H/e^2 and potential.

For the proton-atom channel, the potential includes both that of the nucleus $\mathcal{V}=1/u$ and the surrounding electron cloud [Eq. (22)]. At large distances from the nucleus, $u>>\alpha$, the total potential is well approximated by the quadrupole [Eq. (23)]. For the atom-atom channel, the total potential includes contributions from the proton-proton, proton-electron and electron-electron potentials [Eq. (40)], which is well approximated by the quadrupole-quadrupole formula [Eq. (41)] for large separations.

To calculate the transition probability, we use these quadrupole formulas to approximate the potential for $u>4\alpha$, and for $u<1/2$, we approximate the potential energy between the electron clouds and the electron clouds and the protons by their central values. This both speeds the calculation and reduces the numerical error.

Figure 4 traces the transmission probability for protons to interact with atoms and atoms to interact with atoms at zero relative energy as a function of angle and magnetic field. In the atom-proton case, the protons can most easily penetrate through the mutual potential barrier along the axis of the magnetic field and the penetration probability increases markedly with the strength of the magnetic field. In the atom-atom case, we see that the maximum transmission probability occurs at an angle to the field direction and that with antisymmetrization of the electron density the transmission probability increases dramatically. For the reaction rate estimates that follow we will account for the antisymmetrization energy of the two electron clouds.

To translate this transmission probability into a cross section, we must average $|T|^2$ over a sphere and include the appropriate S factor for the reaction where $S(E)$ is defined as

$$S(E)=\sigma E|T|^2 \approx S_0(1+S_1E). \tag{45}$$

In this way, the strong energy dependence of the reaction cross section is removed. For the reaction $^1\text{H}(p,e^+\nu)\text{D}$, $S_0=4.38\times10^{-25}$ MeV b, and $S_1=11.2$ MeV^{-1} at low energies [6]. The reaction of the less abundant deuterons with protons has a much larger S factor of $S_0=2.5\times10^{-7}$ MeV b and $S_1=27.8$ MeV^{-1} [5].

Given these definitions, the reaction proceeds at a rate of

$$r_{12}=(1+\delta_{12})^{-1}n_1n_2\langle\sigma v\rangle \tag{46}$$

$$=(1+\delta_{12})^{-1}n_1n_2\left(\frac{8}{\mu\pi}\right)^{1/2}$$

$$\times S_0(1+S_1kT)(kT)^{-1/2}|T|^2, \tag{47}$$

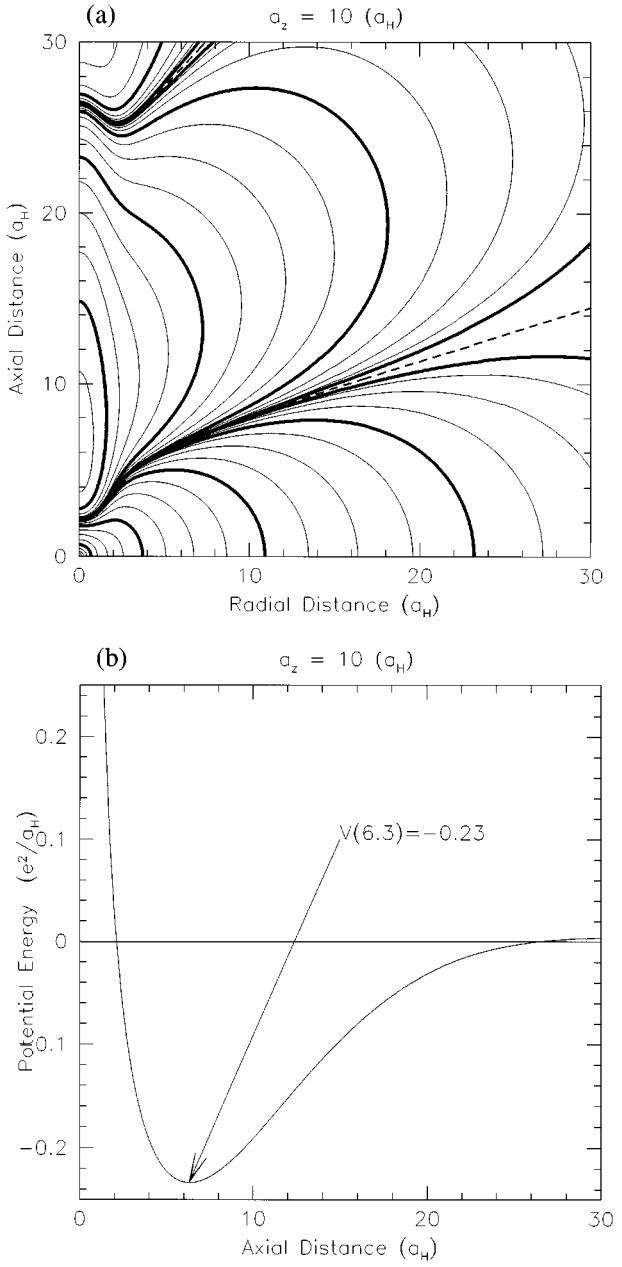

FIG. 3. The figures depict the total potential energy between two magnetized hydrogen atoms including the antisymmetrization energy. For the left panel, the contour spacing is the same as in the right panel of Fig. 1. The right panel illustrates the potential along the axis of the magnetic field.

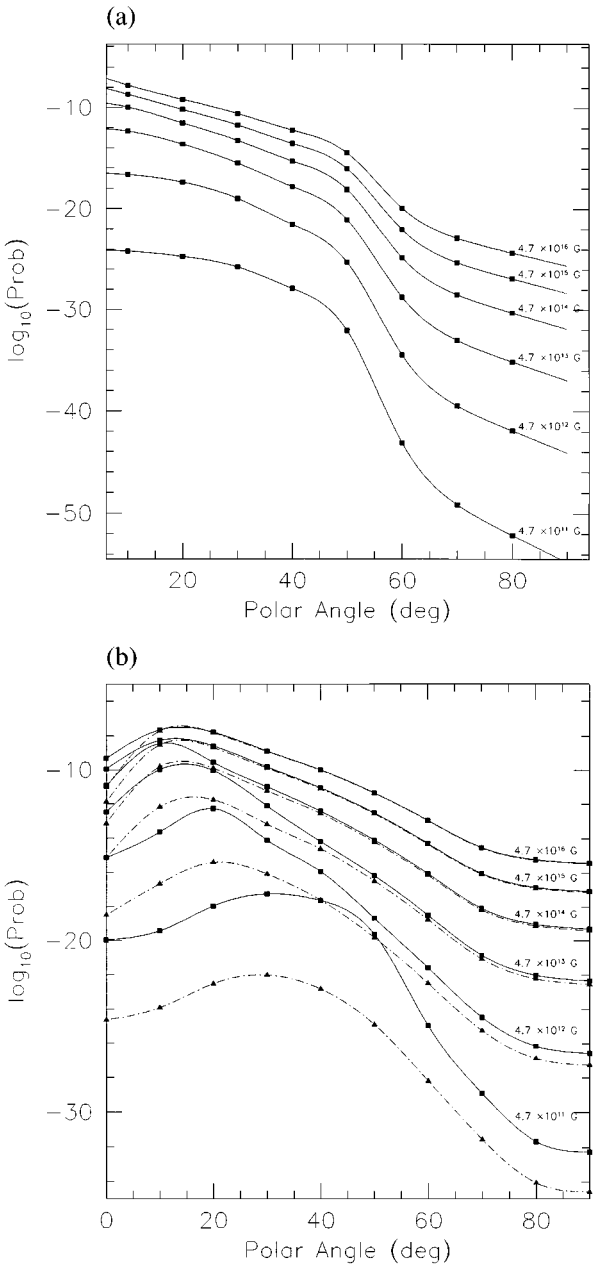

FIG. 4. The left panel depicts the transmission probability as a function of angle and magnetic field for a proton and an atom to interact at zero relative energy. The right panel depicts the same probability for two atoms. The solid lines trace the probability if the antisymmetrization energy of the electrons is considered. The dashed lines show the probability without antisymmetrization.

where μ is the reduced mass of the reactants, and n_1, n_2 are their number densities. r_{12} has the units of reactions per unit time per unit volume, and so we can define a typical time scale for a reactant to be consumed:

$$\tau_{12} = n_1 / r_{12}. \tag{48}$$

We will use this time scale to assess the effectiveness of the screening in catalyzing the nuclear fusion reactions. We also account for the increasing excitation of the gas as the temperature increases and the onset of thermonuclear reactions above several 10^6 degrees.

B. Ground-state fraction

The screening is much less effective if the electron is in an excited state, and so we estimate the fraction of atoms in the ground state by first calculating the ionization equilibrium and then the fraction of neutral atoms in the ground state.

Lai and Salpeter [7] give the form of the Saha equation for hydrogen atoms, electrons, and protons in equilibrium in the presence of a quantizing magnetic field. Throughout this formalism, we use the natural units of the problem; i.e., T is the temperature in units of 3.15×10^5 K, M is the mass of the

system in units of the electron's mass (1840 for hydrogen and 3670 for deuterium), b is the strength of the magnetic field in units of 2.35×10^9 G, and n_g is the number density of the gas in units of $6.76\times10^{24}\,\mathrm{cm}^{-3}$.

We first look at the unexcited hydrogen atom. For the partition function of the ground state in a quantizing magnetic field, Lai and Salpeter [7] give

$$Z_{\mathrm{ground}}(H)\simeq n_g^{-1/3}\left(\frac{MT}{2\pi}\right)^{1/2}\exp\left(\frac{|E(H)|}{T}\right)Z_\perp, \qquad (49)$$

where $E(H)=-0.16l^2$ (the ground-state energy of the atom), $l=\ln b$, and

$$Z_\perp=\frac{n_g^{-2/3}}{(2\pi)^2}\int_0^{K_{\perp\,\max}}2\pi K_\perp dK_\perp\exp\left[-\frac{E_\perp(K_\perp)}{T}\right], \qquad (50)$$

$$Z_\perp\simeq\frac{n_g^{-2/3}}{2\pi}\int_0^{K_{\perp\,\max}}K_\perp dK_\perp\exp\left[-\frac{\tau}{2M_\perp T}\ln\left(1+\frac{K_\perp^2}{\tau}\right)\right] \qquad (51)$$

$$=n_g^{-2/3}\frac{M_\perp'' T}{2\pi}, \qquad (52)$$

where $M_\perp=M+\xi b/l$ (with $\xi\simeq2.8$) and

$$\tau\simeq0.64l\xi b\left[1+\frac{Ml}{\xi b}\right]^2. \qquad (53)$$

Here we have explicitly integrated to $K_{\perp\,\max}$, and so we replace $M_\perp'$ of Lai and Salpeter [7] with $M_\perp''$

$$M_\perp''=M_\perp'\left[1-\left(1+\frac{K_{\perp\,\max}^2}{\tau}\right)^{-\tau/2M_\perp' T}\right], \qquad (54)$$

and $M_\perp'$ is as given by Lai and Salpeter [7],

$$M_\perp'=M_\perp\left(1-\frac{2M_\perp T}{\tau}\right)^{-1}. \qquad (55)$$

As $K_{\perp\,\max}\to\infty$, $M_\perp''\to M_\perp'$ and we recover the Lai-Salpeter [7] result. $K_{\perp\,\max}$ is the upper limit on the perpendicular momentum for the given state. The electron clouds of neighboring atoms should not overlap; otherwise, the gas would become pressure ionized. Therefore, we take the size of the state, $R_K=K_\perp/b<R_g=n_g^{-1/3}$, as the defining condition on $K_{\perp\,\max}$. We obtain

$$K_{\perp\,\max}=bn_g^{-1/3}. \qquad (56)$$

The total partition function of the neutral atom is given by

$$Z(H)=Z_{\mathrm{ground}}(H)z_\nu(H)z_m(H), \qquad (57)$$

where z_ν and z_m are the partition functions for excitations of the ν and m quantum numbers, respectively. Lai and Salpeter [7] argue that the $z_\nu(H)\simeq1$ as these states are hardly occupied relative to the ionized, $m>0$, and ground states. For the contribution of the $m>0$ states to the partition function, they obtain

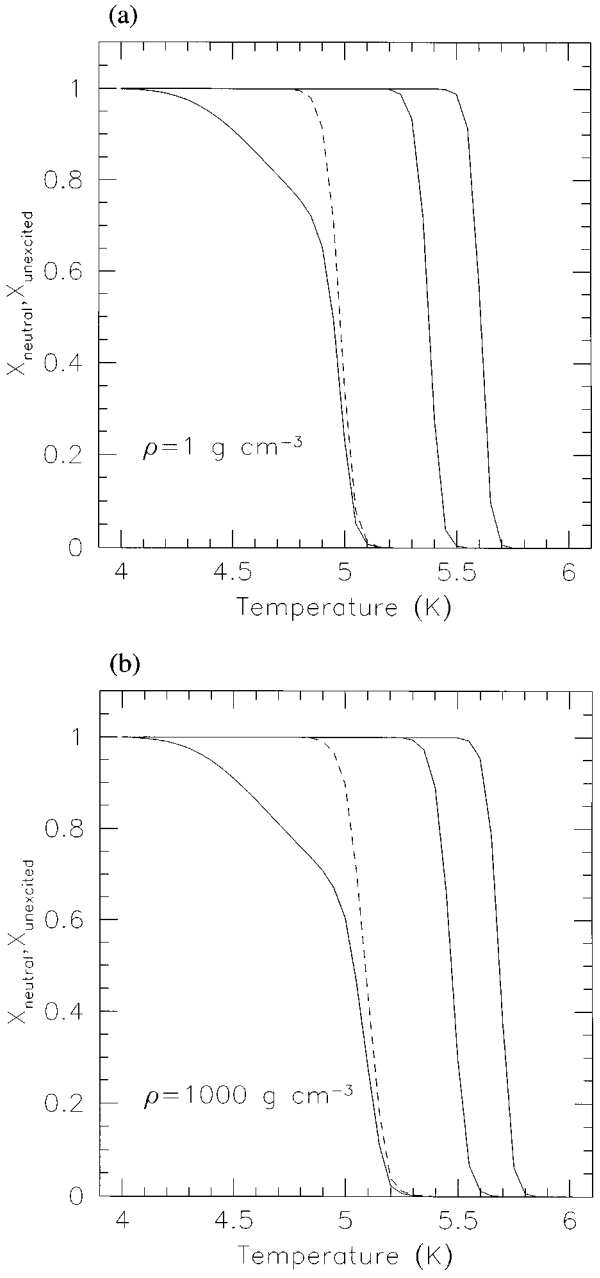

FIG. 5. The ground-state fraction as a function of temperature, density, and magnetic field. The left panel shows the neutral fraction as a dashed line and the unexcited fraction as a solid line for $\rho\sim1$ g cm^{-3} and $B=10^{12}$, 10^{14}, and 10^{16} G. The right panel is for a density $\rho\sim1000$ g cm^{-3}.

$$z_m(H)\simeq(1+e^{-b/MT})\sum_{m=0}^{\infty}\frac{M_{\perp m}''}{M_\perp''}\times\exp\left[-\frac{1}{T}\left(0.16l^2-0.16l_m^2+m\frac{b}{M}\right)\right], \qquad (58)$$

where we have several additional auxiliary definitions

$$l_m=\ln\left(\frac{b}{2m+1}\right), \qquad (59)$$

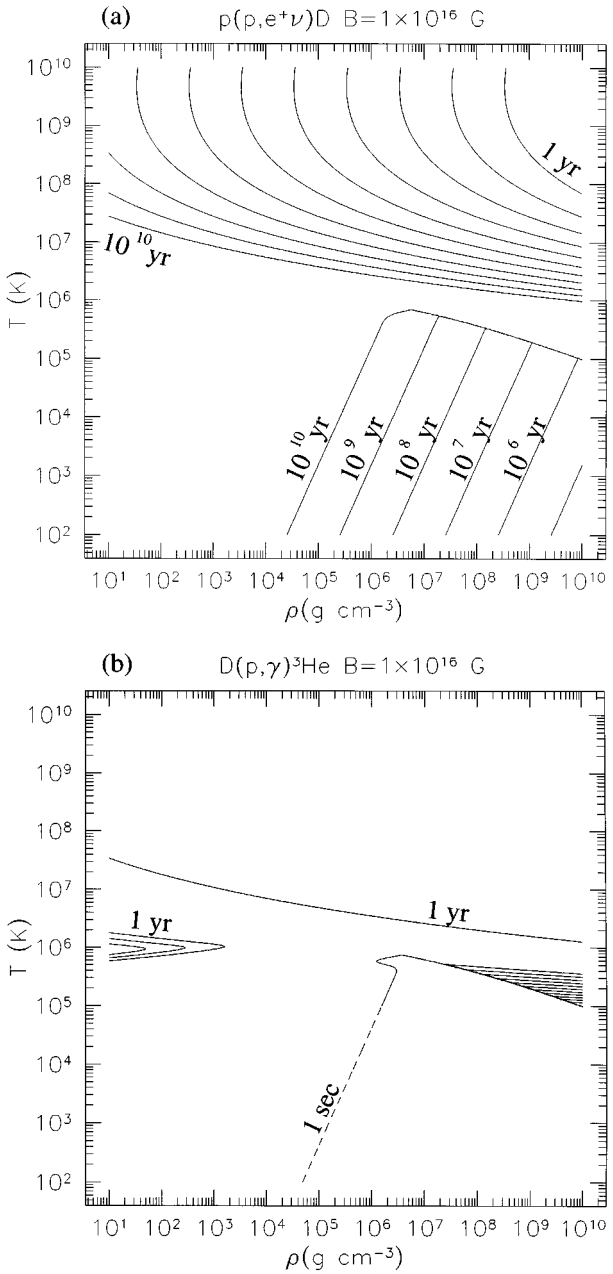

FIG. 6. The two panels depict the reaction time scale for the reactions $p(p,e^+\nu)D$ and $D(p,\gamma)^3$He for $B=10^{16}$ G over a range of temperatures and densities. The dashed contour traces τ of 1 sec. The solid contours trace locii of time scales ranging from 1 year to 10^{10} years with a factor of 10 in between each contour.

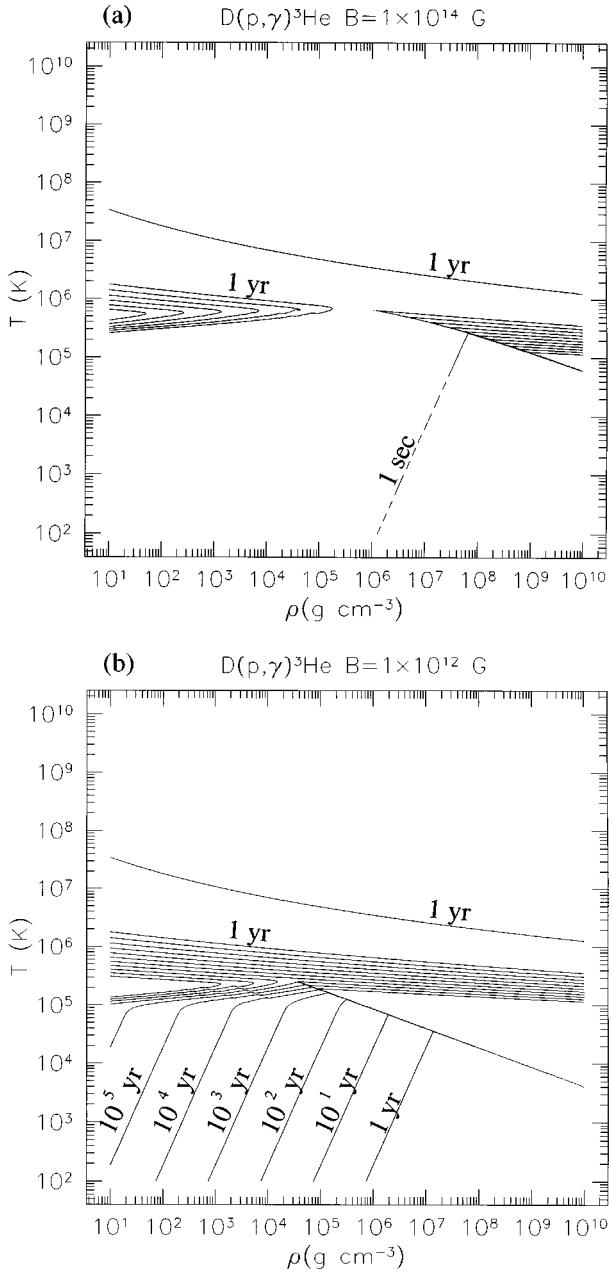

FIG. 7. The two panes depict the reaction time scale for the reaction $D(p,\gamma)^3$He for $B=10^{14}$ G and 10^{12} G over a range of temperatures and densities. The dashed contour traces τ of 1 sec. The solid contours trace locii of time scales ranging from 1 year to 10^{10} years with a factor of 10 in between each contour.

and as with ground state we correct for $K_{\perp\,\max}<\infty$ with

$$M''_{\perp m}=M'_{\perp m}\left[1-\left(1+\frac{K^2_{\perp\,\max}}{\tau}\right)^{-\tau_m/2M'_{\perp m}T}\right] \tag{60}$$

and $M'_{\perp m}$ is as given by Lai and Salpeter [7],

$$M'_{\perp m}=M_{\perp m}\left(1-\frac{2M_{\perp m}T}{\tau_m}\right)^{-1}. \tag{61}$$

$M_{\perp m}$ is given by the relation

$$1-\frac{M}{M_{\perp m}}\simeq\frac{b}{M}\left[\frac{m+1}{b/M+0.16l_m^2-0.16l_{m+1}^2}-\frac{m}{b/M+0.16l_{m-1}^2-0.16l_m^2}\right], \tag{62}$$

and we use the additional definition

$$\tau_m\simeq 0.64l_m(M_{\perp m}-M)\left[1+\frac{M}{M_{\perp m}-M}\right]^2. \tag{63}$$

The ratio of the number of atoms in the ground state to the number of neutral atoms is given by

$$\frac{X_{\text{ground}}(H)}{X(H)} = \frac{Z_{\text{ground}}(H)}{Z(H)} = \frac{1}{z_m(H)}. \tag{64}$$

Next we calculate the ionization-recombination equilibrium:

$$\frac{X(H)}{X_p X_e} = \frac{Z(H)}{Z(p)Z(e)} \tag{65}$$

$$\simeq n_g \left(\frac{b}{2\pi}\right)^{-2} M_\perp'' \left(\frac{T}{2\pi}\right)^{1/2} \tanh\left(\frac{b}{2MT}\right) \times \exp\left(\frac{|E(H)|}{T}\right) z_m(H), \tag{66}$$

where $X(H)=n(H)/n_g$, $X_p=n_p/n_g$, and $X_e=n_e/n_g$ are the number density fractions of the different species.

Combining Eq. (64) and Eq. (66) yields the fraction of ''shielded'' nuclei as a a function of temperature, density, and magnetic-field strength. Figure 5 depicts the fraction of unexcited hydrogen atoms in the gas as function of temperature for several field strengths and two densities.

C. Thermonuclear reactions

We parametrize the thermonuclear reaction rates (e.g., [5]) by

$$r_{pp} = 3.06\times 10^{-37}\ \text{cm}^3\ \text{sec}^{-1} n_p^2 T_6^{-2/3} \exp(-33.71 T_6^{-1/3}), \tag{67}$$

$$r_{pD} = 3.28\times 10^{-19}\ \text{cm}^3\ \text{sec}^{-1} n_p n_D T_6^{-2/3} \exp(-37.11 T_6^{-1/3}). \tag{68}$$

The time scale for the exhaustion of a particular reactant becomes

$$\tau_1 = \frac{n_1}{r_{\text{thermo}} + r_{\text{magneto}}}. \tag{69}$$

Figure 6 shows the reaction time scale for the consumption of hydrogen and deuterium in the reactions $p(p,e^+\nu)D$ and $D(p,\gamma)^3$He, respectively, for a magnetic field of 10^{16} G.

Even in this very strong magnetic field, the p-p reaction proceeds only very slowly below temperatures of 1×10^6 deg; however, over 10^6's of years, the hydrogen gas would be processed to deuterium and then to helium in such a strong magnetic field. It would provide a steady source of energy, while eroding the storehouse of hydrogen which could potentially fuel a thermonuclear runaway. Relatively, the second reaction proceeds instantly with time scales of less than 1 year for the interesting range of densities and temperatures.

For the weak fields depicted in Fig. 7 only the deuterium reaction proceeds at a significant rate.

III. DISCUSSION

We find that in strong magnetic fields ($B\gtrsim 10^{12}$ G), the cross section for nuclear fusion is dramatically larger than in the unmagnetized case. For these strong fields, deuterons fuse to ^{3}He over short time scales ($\lesssim 10^6$ yr) for the density and temperatures expected on the surface of a neutron star. Because of the inherent weakness of the p-p interaction, the fusion of protons to deuterium is only important over cosmological timescales for ultrastrong fields ($B\gtrsim 10^{16}$ G) in spite of the large enhancement in the cross section of this reaction.

For larger atoms ($Z>1$), we expect that reaction cross sections will also be larger in the presence of an intense magnetic field. However, the shielding is unlikely to be as effective as for the $Z=1$ case, because additional electrons must occupy $m>0$ levels which are much less effective at screening the nuclear charge.

[1] L. D. Landau and E. M. Lifshitz, *Quantum Mechanics*, 3rd ed. (Pergamon, Oxford, 1977).

[2] H. Ruder *et al.*, *Atoms in Strong Magnetic Fields: Quantum Mechanical Treatment and Applications in Astrophysics and Quantum Chaos* (Springer-Verlag, New York, 1994).

[3] J. Binney and S. Tremaine, *Galactic Dynamics* (Princeton University Press, Princeton, NJ, 1987).

[4] L. D. Landau and E. M. Lifshitz, *Quantum Mechanics: Non-Relativistic Theory*, 3rd ed. (Pergamon, Oxford, 1989).

[5] D. D. Clayton, *Principle of Stellar Evolution and Nucleosynthesis* (The University of Chicago Press, Chicago, 1983).

[6] J. N. Bahcall *et al.*, Rev. Mod. Phys. **54**, 767 (1982).

[7] D. Lai and E. E. Salpeter, Phys. Rev. A **52**, 2611 (1995).